Comprehensive Untargeted Lipidomic Profiling of Third Generation Lentiviral Vectors and Packaging Cells

Joshua A. Roberts[a], Elena Godbout[b], Jocelyn A. Menard[a], Christopher N. Boddy[c], Jean-Simon Diallo[b, d], Jeffrey C. Smith[a, e, f *]

[a] Department of Chemistry, Carleton University
[b] Centre for Cancer Therapeutics, Ottawa Hospital Research Institute
[c] Department of Chemistry and Biomolecular Sciences, University of Ottawa
[d] Department of Biochemistry, Microbiology and Immunology, University of Ottawa
[e] Institute of Biochemistry, Carleton University
[f] Carleton Mass Spectrometry Centre, Carleton University
* To whom correspondence should be addressed

Keywords: Lipidomics, Lentiviral Vectors, HEK 293T, Biotechnology, Biotherapeutics, Mass Spectrometry

Corresponding Author Information

Email: jeff.smith@carleton.ca. Phone: +1 613-520-2600 ext. 2408

Abstract

Lentiviral Vectors (LV) are emerging tools for genetic therapies and novel cancer treatments. While effective, LV-based therapies have extremely large costs associated with their manufacturing and delivery. LV technology descends from human immunodeficiency virus (HIV), whose lipid envelope has been previously measured and shown to have a direct impact on its transduction efficiency. We developed a rapid, robust, and sensitive untargeted lipidomics pipeline to analyze novel LV biotherapeutic products and demonstrate its utility on HEK 293T packaging cells and concentrated culture media containing LV. The impact of 48 hours of LV production on the lipidome of HEK 293T cells was measured and compared to the expression of Vesicular stomatitis virus G protein (VSV G) over the same timeframe. 151 lipids were identified in HEK 293T packaging cells, 84 of which had fold changes with FDR-corrected $P<0.05$ compared to HEK 293T treated with media. It was found that fold changes with FDR-adjusted $P<0.05$ after VSV G expression and LV production were highly correlated ($R^2=0.89$). Concentrating LV in culture media led to the identification of 102 lipids, half of which being determined to be unique LV virion lipids after subtracting the media lipidome. Our approach can be readily used to study the lipid dynamics of large-scale LV production and be rapidly translated into targeted methods to quantify individual lipid components or applied to other viral vector platforms.

Introduction

Lentiviral Vectors (LVs) are biotechnology tools used to deliver genetic material encoding critical functional proteins engineered from the *Retroviradae* family of viruses, including human immunodeficiency (HIV) 1 and 2. LVs are critical tools in emerging gene and cell therapies due to their wide tropism and in their ability to deliver genes to dividing and non-dividing cell types. Currently, LVs are used in 9.9% of gene therapies undergoing clinical trials world wide[1]. Their ability to infect both dividing and non-dividing cells, stably integrate transgenes into host genomes, and deliver large amounts of genetic material provides flexibility and assurance for both clinical use and research[2,3]. In 2017, Tisagenlecleucel was approved by the U. S. FDA manufactured by Novartis and sold under the name Kymriah to treat relapsed acute lymphoblastic leukemia (ALL) in patients up to 25 years old[4,5]. While Tisagenlecleucel is very effective, it also has a very high cost of $475,000 USD per dose[6]. Manufacturing this biotherapeutic product under current good manufacturing processes (GMP) requires as many as 9 steps with specialized facilities and equipment[7]. LVs are typically produced using adherent HEK 293T cells[8,9] in bioreactors to achieve the high titers required for transduction[10].

Studies exploring the origins and properties of the HIV-1 lipid envelope, which third generation LV technology is descended from, have been published over the course of several decades. The lipid dynamics associated with the production and transduction of third generation LV remain unreported. In 1985, it was discovered that HIV-1 derives its lipid envelope from the host cell's plasma membrane as it buds away[11]. Later, it was found that the HIV-1 envelope is also enriched in cholesterol and specific classes of phospholipids compared to the host cell, creating a highly ordered membrane[12,13]. In the

early 2000s, liquid chromatography mass spectrometry (LCMS) instrumentation and additional techniques were used to show that the HIV-1 envelope was comprised of phosphatidylcholine (PC), phosphatidylserine (PS), phosphatidylinositol (PI), sphingomyelin (SM), and cholesterol, forming from coalescing lipid rafts on the host plasma membrane[14–16]. However, the composition of the HIV-1 viral envelope is critical for efficient transduction of host cells[15,17,18]. This suggests lipid composition of clinical grade LV should be monitored as a means of quality assurance for the final product or as a strategy to optimize the manufacturing process and lower production costs.

Advancements in LCMS technology and data processing pipelines have enabled the efficient realization of novel lipidomics analysis techniques. LCMS instruments are highly sensitive and automated enabling high-throughput analysis using small amounts of sample, which is critical for LV due to their high cost of manufacturing. Using untargeted lipidomics platforms, it becomes possible to identify and quantify hundreds of lipids in a single sample and gain a thorough understanding of the dynamic characteristics exhibited by lipids.[19] The Lipid MAPS structure database currently contains 47581 unique lipids and continues to grow with new lipid structures being reported each year[20]. In silico databases like Lipid Blast[21] and Lipid Match[22] provide automated, high-throughput searching of tandem MS spectra and dramatically reduce the time spent identifying large numbers of peaks created by feature finding tools. Comprehensive and reproducible pipelines for lipidomic profiling have been demonstrated for human plasma[23] and cell culture[24,25]. Lipidomics studies for biomarker discovery and lipid signatures have been applied to Alzheimer's[26] and Parkinson's[27] disease cohorts, toxicological studies[28], as well as several cancer groups such as cervical[29] and prostate[30]. Lipidomics workflows typically

use Bligh-Dyer[31], Folch[32], or Matyash[33] methods, and HPLC separation using C18 columns. Mobile phases typically consist of water and isopropanol, with acetonitrile and methanol also being commonly employed[34]; volatile ammonium salts, such as ammonium formate, acetate, and fluoride are usually added as well to improve separation and improve ionization of neutral lipids[35]. Efforts to standardize and implement “best practices” for lipidomics sample preparation, data acquisition and data processing have been proposed[36] and have been tested on various LCMS platforms and laboratory environments[37,38] to provide guidance and ensure consistency in the lipidomics community.

With the emergence of new genetic therapies and their pursuit of approval, it is increasingly important to incorporate lipidomics and targeted lipid analysis as a crucial quality control measure for clinical-grade LVs as lipid envelope composition is shown to be critical for efficient transduction. In order to meet this requirement, we present a comprehensive lipidomics method that focuses on HEK 293T packaging cells and LVs. By employing this method, we can reveal and understand the lipid dynamics involved in the production of high-titer clinical-grade LVs using bioreactors. This work enhances the understanding of biomanufacturing techniques and holds the potential to be employed as a quality control metric during the manufacturing of biological therapies.

Experimental Section

Chemicals and Materials: Fetal bovine serum (FBS), dimethyl sulfoxide (DMSO), phosphate buffered saline (PBS), 4-(2-hydroxyethyl)-1-piperazineethanesulfonic acid (HEPES), ViraPower LV plasmid set, OPTI-MEM and Optima LCMS grade solvents (water, methanol and isopropanol) were purchased from Fisher Scientific (Ottawa, ON), sodium acetate, ammonium formate and myriocin were purchased from Sigma-Aldrich (St. Louis, MO/Mississauga, ON, Canada). Chloroform was purchased from Caledon Laboratories Ltd. (Georgetown, ON, Canada). Dulbecco's Modified Eagle Medium (DMEM) was purchased from Corning (Corning, NY, USA). Synthetic lipid standards lysophophatidylcholine (LPC) 13:0, lysophosphatidylethanolamine (LPE), phosphatidylcholine (PC) 19:0/19:0 and cholesteryl ester (CE) 17:0 were purchased from Avanti Polar Lipids, Inc. (Alabaster, AL, USA). Polyethyleneimine (PEI) was purchased from VWR (Mississauga, ON, Canada).

Cell Culturing: HEK 293T cells were cultured in 6-well plates or in T75 flasks in DMEM supplemented with 10% FBS, 34 mM HEPES, 100 µg/ml penicillin and 100 µg/ml streptomycin for 48 hr with 70-90% confluency at 37°C. For myriocin-treated samples, myriocin was dissolved in DMSO and added to culture media at 10 µM, then incubated for an additional 48 hr. For LV production, transfection mix was prepared with pLP1, pLP2, pLENTI VSV-G and pLENTI FL (Fluc transgene) plasmids in OPTI-MEM:PEIpro at a 1:1 µg DNA to µL PEIpro and incubated for 15 min before adding to 6-well plates or T75 flask culture media. For HEK 293T cells cultured in 6-well plates, the following steps were performed: samples were centrifuged in the plates at 900 x g for 5 minutes, the culture media was removed from each well, and the cells were washed twice with 2 mL of PBS.

Cells were scraped into 500 µL PBS and transferred into microtubes; PBS was removed from the cells by centrifugation (900 x g, 4 min). Cell pellets were snap-frozen with dry ice and stored at -80°C until lipids were extracted. To harvest LV for lipidomics, culture media was removed from T75 flasks and duplicate flasks were pooled together, then centrifuged at 900 x g for 10 min. The supernatant was subjected to ultracentifugation at 76653 × g and 4°C for 90 min. Pelleted LV was reconstituted in 110 µL OPTI-MEM media and stored at -80°C until analysis.

Lipid Extractions: Lipids were extracted using a modified Bligh-Dyer protocol[39,40]. Briefly, pellets were removed from storage and transferred to conical 10 mL glass centrifuge tubes (Kimble 73785-10). A matrix blank and 125 µL FBS were also extracted as quality assurance samples. 1 mL water with 0.1 M sodium acetate and 2 mL methanol with 2% acetic acid (v/v) were added to each tube followed by bath sonication for 5 min. A solution of lysophophatidylcholine (LPC) 13:0 (10 µM), lysophosphatidylethanolamine (LPE) 13:0 (20 µM), phosphatidylcholine (PC) 19:0/19:0 (10 µM) and cholesteryl ester (CE) 17:0 (20 µM) was prepared in chloroform and 40 µL was spiked into each sample. The final concentrations were 1.6 µM for LPC 13:0 and PC 19:0/19:0 and 3.2 µM for LPE 13:0 and CE 17:0 in each sample. 1.5 mL chloroform was then added to each tube and shaken for 2 min, then centrifuged (528 x g, 2 min). The chloroform layer was carefully removed by Pasteur pipette and transferred to a new 10 mL glass centrifuge tube. The water/methanol layer was then extracted two more times with 1 mL chloroform with each chloroform layer combined with the previous extractions for a total of 3.5 mL per sample. The chloroform was then evaporated under a stream of nitrogen and 250 µL of 45:45:10 methanol, ethanol and toluene was added to each tube, vortexed, incubated at 30°C for 10 min,

centrifuged (528 x g, 2 min) and transferred to an amber HPLC vial with a 250 µL glass insert. For pelleted LV samples, the 250 µL was further concentrated to 85 µL.

Titer Determination: Titers were determined using a high-throughput assay based on Fluc transgene expression.[41] Briefly, HT1080 cells were cultured in a 96-well plate at a seeding density of $5x10^3$ cells/well. Dilutions of a standard LV-Fluc stock were prepared in cell culture media at concentrations ranging between $5x10^4$ LV/mL and $5x10^7$ TU/mL. HT1080 cells were transduced with the LV standard dilutions or with the media containing harvested LV-Fluc, centrifuged at 900 x g for 5 min and incubated for 72 hr; luminescence readings were then taken for each sample. A standard curve was constructed by plotting luminescence values for the 4 LV stock dilution wells with the LV concentration (Supporting Figures S1). The resulting linear equations were used to determine experimental titers.

Data Acquisition: Additional LCMS method parameters are outlined in the Supporting Information. All data were acquired on an Agilent 6546 QToF mass spectrometer with an Agilent 1260 HPLC. An Agilent Poroshell 120, EC-C18 2.7 um, 2.1x100 mm column heated to 45°C was used for analyte separation, 5 and 10 µL injection volumes were used for positive and negative polarities, respectively. Injections were separated using a binary mobile phase gradient, solvent A contained water:methanol (1:1 v/v) with 10 mM ammonium formate, and solvent B was methanol:isopropanol (1:3 v/v) with 10 mM ammonium formate. The flow rate was constant at 0.4 mL/min, injections in positive polarity used the following HPLC gradient program: 0 min 20% B, 0.35 min 20% B, 0.4 min 32% B, 9.6 min 44% B, 9.7 min 65% B, 11.5 min 65% B, 26.8 min 82%, 27.3 min 87% B, 37 min 96% B, 37.1 min 100% B, 44 min 100% B. Injections in negative polarity

used a modified gradient program: 0 min 20% B, 0.35 min 20% B, 0.4 min 32% B, 9.6 min 44% B, 9.7 min 65% B, 11.5 min 65% B, 30.0 min 86% B, 30.1 min 100% B, 39 min 100% B. The HPLC was run at 20% B for 5 minutes following each injection to re-equilibrate the column. Technical triplicates for each sample in both polarities were recorded. Blank samples of methanol were analyzed every 15 injections to ensure sample carry-over was not observed and an in-house standard of FBS extract was also injected at the same interval as a positive quality control check. Once triplicates were recorded for each sample in both polarities at the MS-level only, replicates for each sample were pooled together and analyzed using a data-dependent analysis (DDA) method with the iterative injections feature activated.

Data Analysis: Complete LCMS data processing parameters are outlined in the Supporting Information. Lipids were identified in pooled samples using Agilent Lipid Annotator with the software default settings. A list of abbreviations for all lipid classes detected in the analysis is provided in Supporting Table S1. MS-level only data files were converted to mzML format using MSConvert[42] and imported into MZmine 3.3.0[43]. All files were processed with the “Mass detection” module using the centroid detector. Identified lipids were extracted from the MS-level data using the “Targeted feature extraction” module. Feature list retention times (RTs) were normalized using the “Retention time calibration” module and then aligned using the “Join Aligner” module. The steps were performed on files for each polarity separately, then peak areas were exported from MZmine and combined into the same feature list. Features were removed from the dataset following the “modified 80% rule”[44], where features are only kept if they are detected in 80% of samples from at least one treatment group. Feature lists were then

imported into R (R-4.0.3) normalized with normalizeCyclicLoess[45–48], and batch corrected using removeBatchEffect both from the Limma Package (ver. 3.46.0). For HEK293T samples, missing values were imputed using the Quantile Regression Imputation of Left-Censored (QRILC)[49] method impute.QRILC from the imputeLCMD[50] package (ver. 2.1). *P* values were calculated using Microsoft Excel. FDR correction of *P* values was applied using p.adjust in R. For LV data, missing values were zero-filled and the normalized non-log_2-transformed values from the culture media blank were subtracted from the LV-containing media. Any values which became 0 or negative after this step were removed from the dataset.

Results and Discussion

Considering the significant role of the lipid envelope in HIV transduction, it is crucial to gain a comprehensive understanding of the lipid dynamics involved in the manufacturing process of LVs. This knowledge will play a crucial role in assessing the quality of large batches of LV used in therapeutic applications. Methods commonly used for determining LV titer in biomanufacturing contexts include qPCR[51,52], p24 quantification by ELISA[53,54] and flow cytometry[10]. Vector copy number is also monitored to determine the risks associated with gene delivery and determine the therapeutic benefits for the treatment after LV transduction is completed[55]. Additional methods to assess the quality of clinical-grade LV are not currently employed in large scale LV manufacturing. There is a need for technologically advanced analytical techniques like LCMS to characterize additional aspects of the LV product including the identities and quantities of lipids incorporated into the particles.

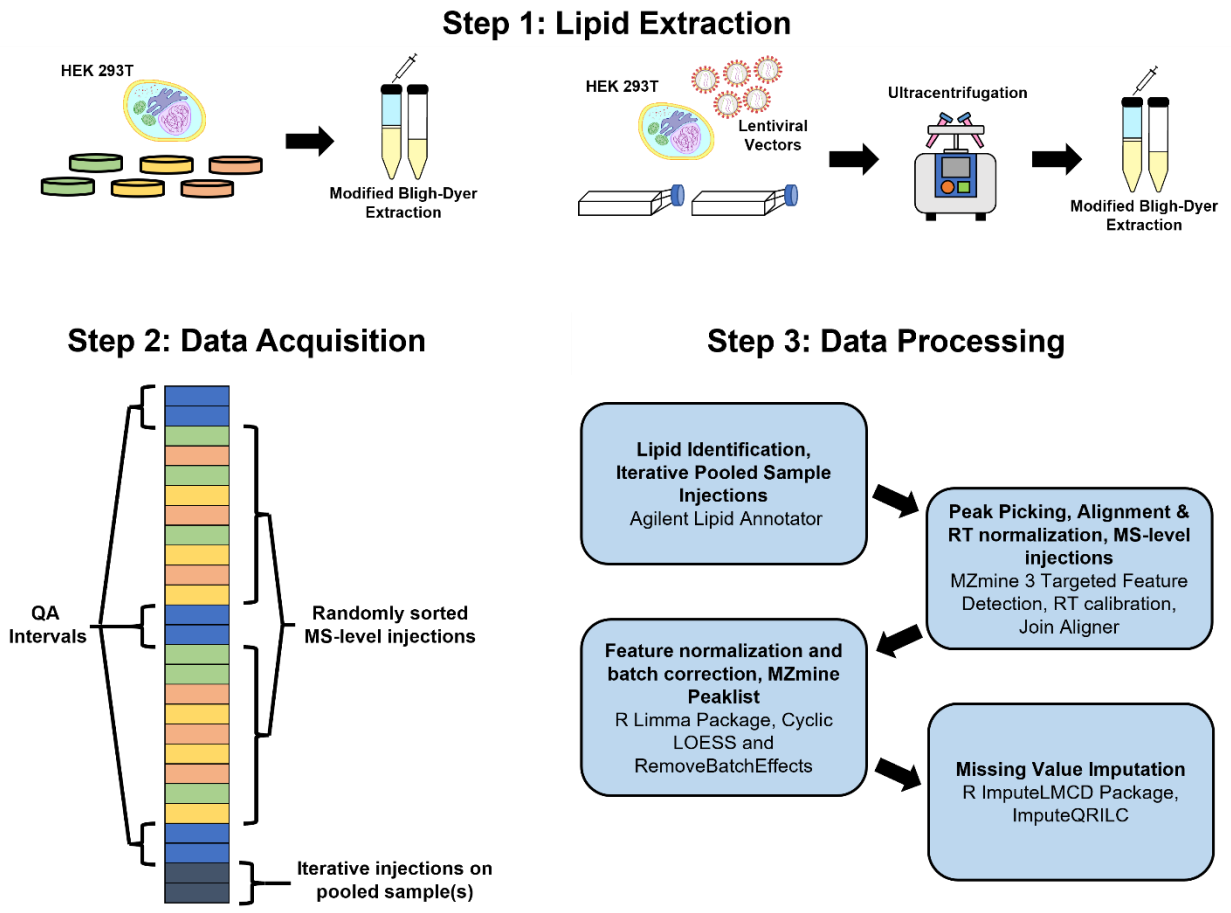

Figure 1. Workflow used to determine the lipidomic profile of third generation LV and packaging cells

To assess the lipid dynamics of LV production, a comprehensive LCMS lipidomics pipeline was developed (Figure 1). Lipids can be extracted using a number of protocols, however a modified Bligh-Dyer extraction[40] was selected due to its ability to extract a wide variety of lipid classes with high-yields[56]. Once lipids were extracted from samples and prepared for LCMS analysis, they were injected in triplicate in random order. A visual representation of a batch is shown in Figure 1. Injections were first performed at the MS-level only to maximize the number of data points along extracted ion chromatograms (XICs) and improve quantification. Methanol blanks were injected at regular intervals

between 10 and 20 injections depending on batch size to assess sample carry-over. A matrix blank and a sample of FBS were also extracted with every batch to determine false positive identifications in samples and to assess instrument performance. A complete list of lipids identified in FBS is shown in Supporting Table S4, as well as a dilution series of FBS extractions to assess the linear response range of the MS (Supporting Table S3 and Supporting Figure S3). 58 lipids were included in the FBS dilution series. The intensities of these lipids span 5 orders of magnitude and had an average RSD of 16.4%. 62% of lipids included in the series had R^2>0.99 and 80% of lipids had R^2>0.97, showing a wide linear dynamic range, allowing for the relative quantification of large amounts of spectral features. FBS extracts were injected at regular intervals during the batch with methanol blanks, as done previously[23–25]. Synthetic standards were also monitored in each injection during the batch to determine mass accuracy, retention time drift and signal intensity drift for feature extraction parameter optimization[36]. While other targeted instrument platforms may provide greater sensitivity, untargeted approaches such those described here acquire data and allow systematic analysis without any prior information about the sample[57]. Thus, hypotheses can be generated from these datasets that may be translated to validated and targeted methods in subsequent experiments.

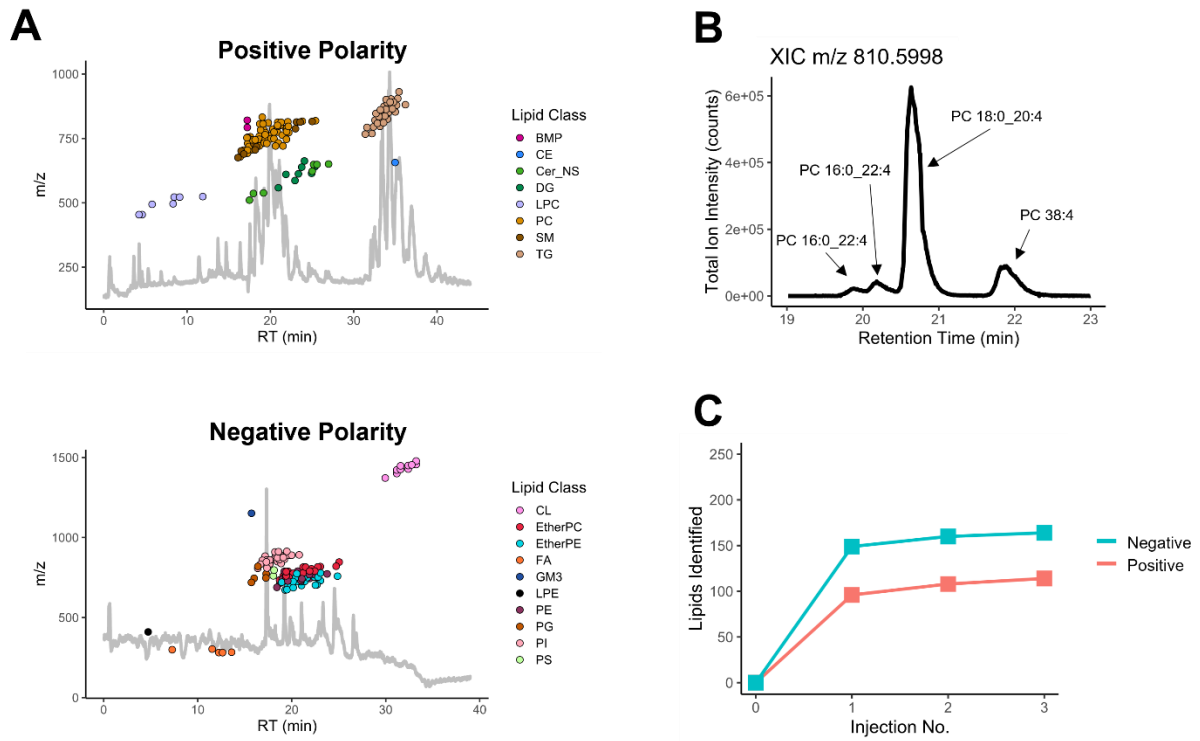

Figure 2. The lipidome is comprehensively examined using both positive and negative polarities, long HPLC gradients, and iterative injections with rolling exclusion lists. A) Characteristic two-dimensional maps (m/z vs RT) of extracted MS features overlaid with total ion chromatograms (TICs) from pooled HEK 293T lipid extracts treated with 10 µM myriocin processed through our workflow in both positive and negative ionization mode. B) XIC of m/z 810.5998 from FBS revealing four distinct PC species, demonstrating the functionality of our optimized HPLC gradient. C) Relationship between the number of iterative injections for pooled samples and the number of lipids identified.

Once MS-level data were acquired, pooled samples from each treatment group were injected in positive and negative polarity using a data-dependent acquisition method to identify each lipid species. The lipid identifications were formulated into a target list, which was then used for feature extraction on the MS-level samples. As a result, only an untargeted feature extraction step was performed on the pooled samples[58]. This dramatically reduced the complexity of the final dataset as only peaks from identified lipids were used in the data processing pipeline in contrast to typical untargeted lipidomics or metabolomics experiments, which consists of thousands of features[59]. Normalization of

the dataset was achieved using Limma's cyclic LOESS method, which has been found to perform well on benchmark datasets[47,48,60]. Batch-effects were also corrected using the Limma package as a strong difference was observed between FBS extractions from repeats of the same experiment when examined by PCA (Supporting Figure S4). To improve the accuracy of the missing value imputation step, the modified 80% rule was performed on the final dataset to reduce the number of missing values, while still maintaining differential metabolites[61]. A missing not-at-random strategy was employed to impute missing values as the targeted feature m/z and RT extraction parameters were based on the evaluation of standards monitored throughout the batch, and identities were assigned from a pooled sample. Features that were not detected were assumed to be below instrument's level of detection, which was manually set in the targeted feature extraction module of MZmine. The QRILC method was selected to impute missing values as it has been shown to perform well on validated datasets[49]. MS-level scans in both positive and negative polarities were performed sequentially for each sample rather than switch between single injections or use rapid polarity switching within a method to improve quantification and maximize coverage of the lipidome. Annotations for each polarity are shown in a representative pooled sample of HEK 293T cells in Figure 2A, highlighting the coverage obtained using both polarities. Longer HPLC gradients are beneficial for separating lipid isomers in untargeted lipidomics workflows[23]. An XIC of m/z 810.5998 ± 10 ppm in FBS produces 4 resolved peaks, each identifying as PC isomers with the sum composition of 38:4 using Lipid Annotator (Figure 2B). Novel ion mobility instruments have been introduced and applied to untargeted lipidomics experiments, reducing analysis times and enhancing the separation of lipid isomers[62]. However, these platforms

are much less common, more expensive, and are less validated than traditional HPLC platforms[62]. To further increase lipidomic coverage, the iterative injections feature was implemented for the pooled samples. This feature enabled deep lipid identification coverage in a given sample without the need for selecting large numbers of precursor ions for MSMS in each DDA cycle. As a result, fewer precursors were selected per DDA cycle, thus increasing the quality of MSMS spectra used for annotation as relatively more time was spent accumulating transient spectra[63]. With 10 precursors selected per survey scan, there were no additional lipids identified in HEK 293T cells after 2 injections (Figure 2C). Therefore, 2 iterative injections were performed per polarity for each pooled sample.

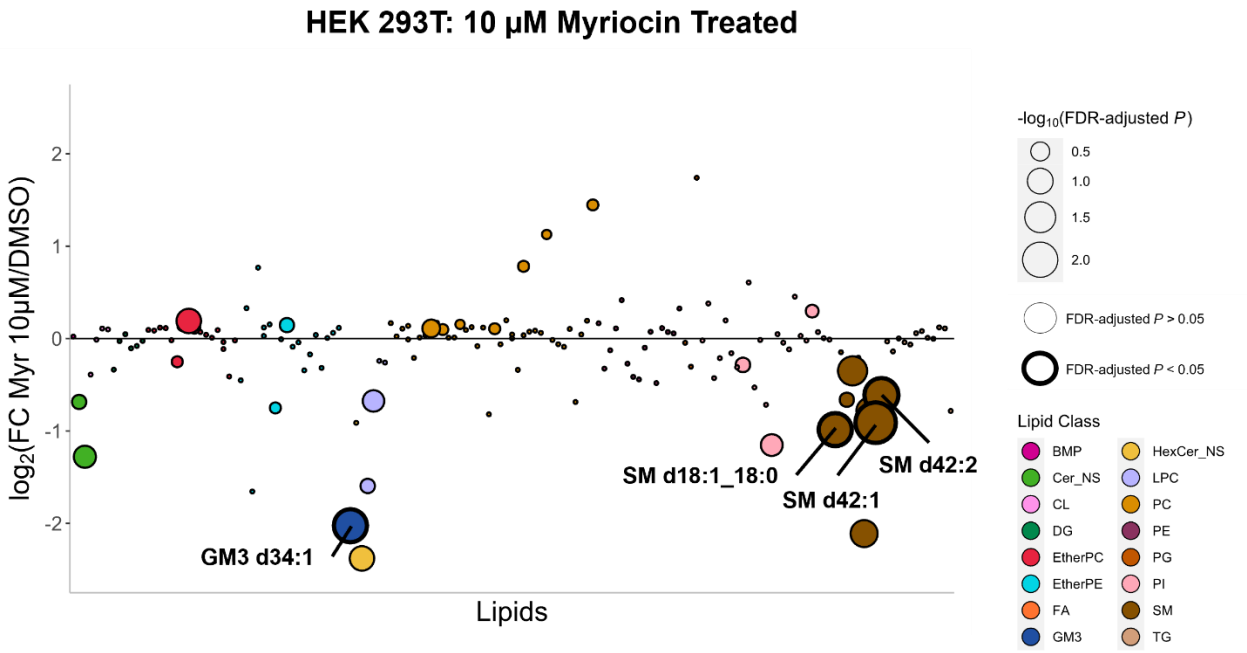

Figure 3. Validation of the lipidomics workflow using HEK 293T cells treated with 10 µM myriocin for 48 hr. Bubble plot of the log_2 fold change of lipids identified in HEK 293T cells treated with 10 µM myriocin compared to a DMSO vehicle control. Significant lipid fold changes are bolded and labeled, confirming anticipated decreases in GM3 and sphingomyelin lipid species.

To validate our pipeline, the lipidomic effects of treating HEK 293T cells for 48 hr with myriocin, a fungal toxin which inhibits the *de novo* synthesis of ceramides by blocking serine palmitoyltransferase, was investigated. Previous lipidomics experiments have shown ceramide-containing lipids decrease after myriocin treatment[64,65]. Using two iterative injections in each polarity, 158 lipids were included in the results after data processing; 73 were in positive polarity and 85 in negative polarity (Supporting Table S6). Following treatment with 10 µM myriocin, significant decreases were observed in several sphingomyelin species (SM) and a single monosialodihexosylganglioside (GM3) compared to vehicle control (DMSO) treated HEK 293T (Figure 3). While previous results showed ceramide species (Cer_NS), hexosyl ceramide (HexCer_NS) also decreased

after myriocin treatment[64], only complex sphingolipid classes were found to be disrupted at 10 µM myriocin. Treatment with 2.5 µM myriocin showed no significant differences compared to DMSO-treated cells (data not shown). HEK 293T cells treated with both 2.5 and 10 µM myriocin were viable after 48 hr as determined by resazurin assay (Supporting Figure S2A). Our data acquisition strategy and data processing workflow were successful in demonstrating previously known lipidomic perturbation as a result of myriocin treatment. As a result, our complete protocol indicated that the approach is efficient to accurately detect biological variation in lipids.

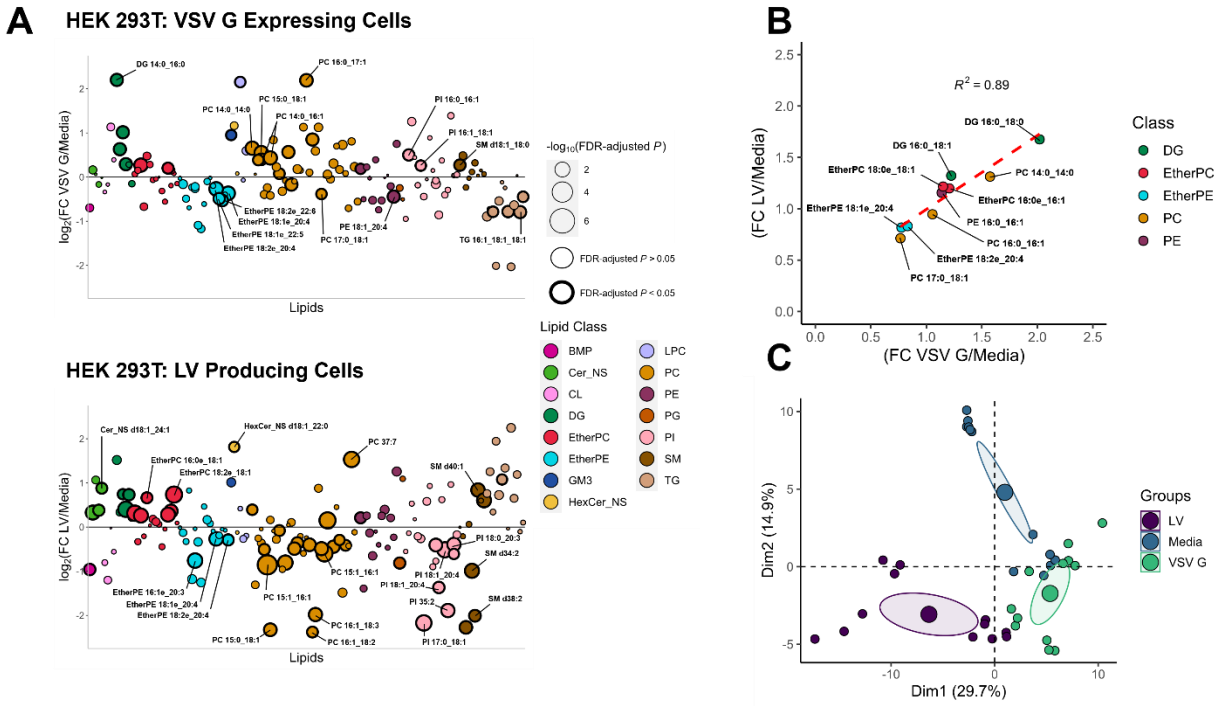

Figure 4. LV-producing HEK 293T undergo significant changes in lipid abundances after 48 hr. A) Bubble plot of HEK 293T VSV G-expressing cells and LV-producing cells after 48 hr compared to control HEK 293T (media). B) Correlation plot between fold changes of LV and VSV G, containing only the lipids that have significant fold changes in both treatments. C) Principal component analysis between the two treatment groups (LV & VSV G) and the control group (media).

A complete untargeted lipidomics experiment was performed to monitor the effects of 48 hr of LV production on the HEK 293T lipidome (Figure 4). As a control, the Vesicular

stomatitis virus G (VSV G) protein, which third generation LV are pseudotyped with, was also expressed in HEK 293T cells, as VSV G can cause extracellular vesicle secretion[66–68]. HEK 293T cells were determined to be viable after 48 hr of VSV G expression or LV production compared to control (media treated) cells (Supporting Figure S2B); LV titers were determined to be 1.25E6 LV/mL (Supporting Table S2). Among the three treatment groups, 151 lipids were included in the results after data processing, 75 in positive polarity and 76 in negative polarity (Supporting Table S5). 51 lipids were found to have significant (FDR-corrected $P<0.05$) fold changes after LV production, 33 lipids were found to have significant fold changes after VSV G expression. Comparing bubble plots examining the fold changes of lipids after VSV G expression compared to control HEK 293T, increases in PC and diacylglycerol (DG) species were observed, while ether-linked phosphatidylethanolamine (Ether PE) and triacylglycerol (TG) species were decreased (Figure 4A and Supporting Figure S6). Many lipids with short fatty acyl chains were found to be increased after VSV G production: PC 14:0_14:0, PC 14:0_16:0, PC 14:0_16:0 and DG 14:0_16:0 (supporting Figure S6). Consistently, PE and ether PE species with polyunsaturated acyl chains (20:4, 22:5 and 22:6) were found to be decreased after 48 hr of VSV G expression. After 48 hr of LV production, Cer_NS, HexCer_NS, DG and ether-linked PC (Ether PC) species were found to be increased, while PC, ether PE, PI, and SM species showed a marked decrease overall (Figure 4A and Supporting Figure S7). These lipid subclasses were found to be highly enriched in the HIV envelope[15,16,18], and suggests they are likely depleting from the HEK 293T plasma membrane during LV production. Consistent with VSV G expression, many lipids with polyunsaturated acyl chains also had negative fold changes (20:4, 22:5, 22:6) from the ether PE and PI

subclasses (Supporting Figure S7). Several lipid species with negative fold changes were identified with odd-chain fatty acids (15:0, 17:7, 17:1, 19:1) from the PC and PI subclasses. Long monounsaturated and saturated ceramide and sphingomyelin species were found to be increased after LV production, contrary to previous findings in HIV membranes[15]. Only 11 lipid species were identified with significant fold changes in both VSV G and LV production conditions, suggesting alternative mechanisms of action on the HEK 293T lipidome (Figure 4B and Supporting Table S8). A strong correlation (R^2=0.89) was observed between the 10 common significant lipid species between both LV and VSV G treatments, suggesting that any lipid changes due to extracellular vesicle secretion may also be implicated in LV production or that the same lipid remodeling pathways are used by the cell to maintain homeostasis under each condition. PC 16:1_18:2 decreased in abundance (FC=0.2) after LV production but increased in abundance (FC=1.8) after VSV G production (Supporting Figure S8); it was removed from the correlation analysis as it was deemed an outlier. When lipid profiles were compared by principal component analysis (PCA), clear separations between LV, VSV G, and Media (control) groups were observed. This would suggest that the lipid dynamics of LV production are not associated with aberrations due to VSV G expression in HEK 293T cells (Figure 4C).

Although monitoring the lipidomic dynamics in packaging cells associated with LV production provides a detailed overview of the processes involved in manufacturing clinical-grade LV, a comprehensive lipidomic analysis of the final LV product would yield crucial insight from a quality control perspective. To study the lipid composition of the LV product itself, HEK 293T cells were cultured in 15 mL T75 flasks (Figure 1) with titers averaging 4.53E7 LV/mL (Supporting Table S1) and two flasks were pooled together for

each lipid extraction to provide enough abundance for the analysis. Concentration of LV from culture media was achieved by ultracentrifugation at 76653 × g for 90 min, which produced a small pellet that was resuspended in OPTI-MEM media. The same volume (110 µL) of OPTI-MEM media was analyzed in isolation using our pipeline to determine if any lipid contamination could be introduced at the pellet resuspension stage. No lipids were identified in either positive or negative polarity when searching the two data-dependent acquisition files with iterative injections (data not shown) and had a similar TIC to a methanol blank (Supporting Figure S5). To determine the background lipid profile of the serum-containing culture media used to grow and maintain HEK 293T during LV production, the same number of untransfected HEK 293T cells were seeded in parallel T75 flasks and incubated for 48 hr. After centrifugation and extraction, this media blank sample was incorporated into the lipidomics analysis and pipeline. The difference in TICs show that LV production creates a large increase in lipid abundances compared to culture media from untransfected cells and suggests that this method allows for the characterization of the LV product (Figure 5A).

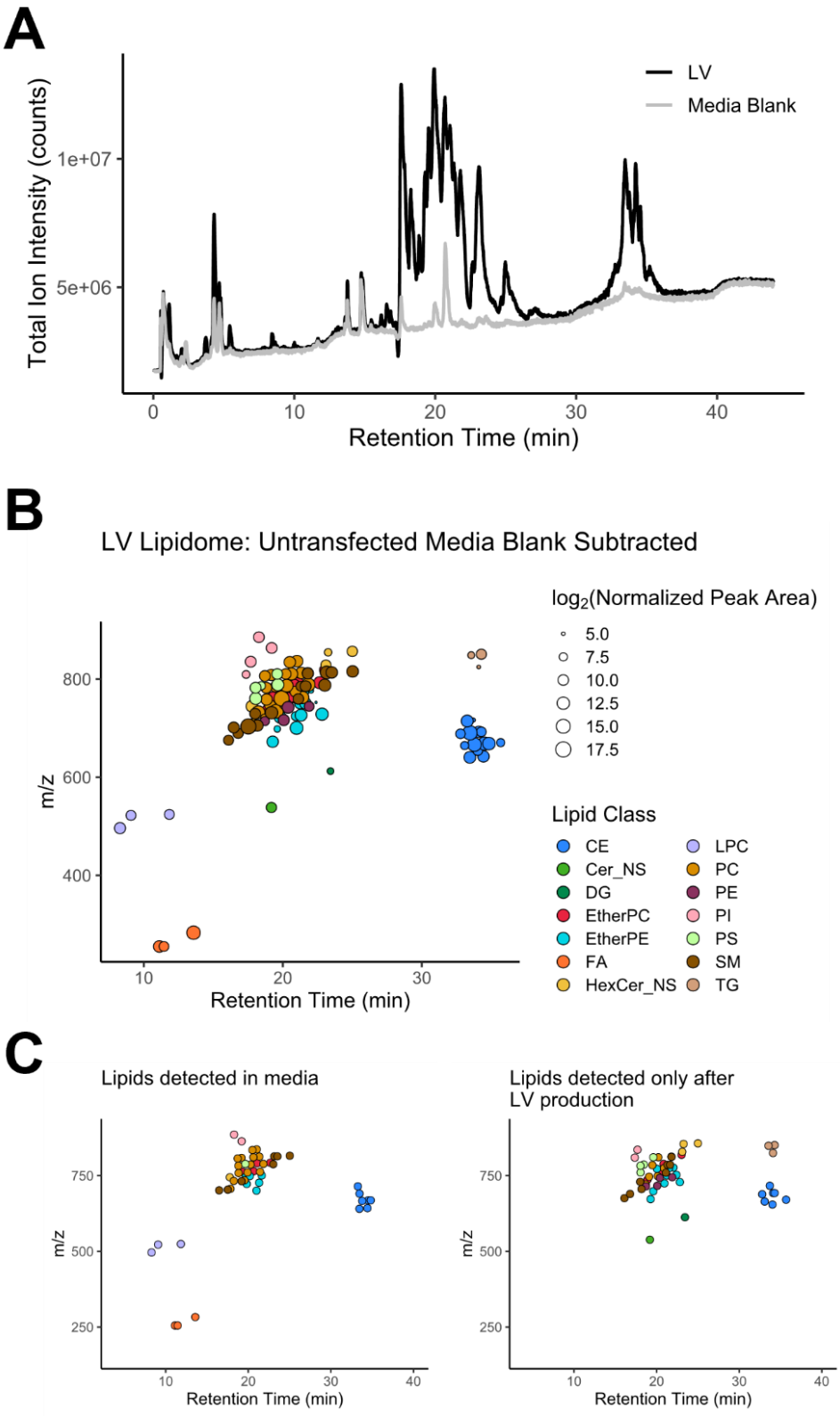

Figure 5. The LV lipid profile was obtained by subtracting the lipid profile of untransfected culture media; many neutral lipids were detected in LV. The lipid

profile of LV was obtained after 48 hr of production in HEK 293T cells. A) TIC of untransfected cell media (grey) from HEK 293T cells overlaid with a TIC of the LV lipidome (black). B) Scatter plot showing identified lipid features and their log_2-normalized peak areas from LV after the untransfected media lipid profile was subtracted. C) Scatter plots showing the annotated lipids in untransfected culture media and the lipid features that are only detected in LV.

To determine the composition of the LV product, a background subtraction strategy was employed to highlight key lipids associated with LV. One software-based approach, called BLANKA, was proposed by Cleary, et al. to highlight differentially expressed metabolites in microorganisms cultured in liquid or solid media with high background signal caused by peptides, sugars and lipids[69]. Using BLANKA, a background media sample is selected and the m/z intensities at each MS scan in the background are subtracted from the biological sample's MS scans at the same timepoint. While BLANKA was not directly used in this present study, a similar approach was used to subtract the background signal from LV data files. Once all media background and LV datafiles were processed using the pipeline described above, the average peak areas of lipids identified in the media were subtracted from the LV samples. Any lipids that had peak areas less than zero were removed from the analysis. Media blanks and LV replicates were normalized separately to avoid artificially increasing the peak areas of lipids identified in the media, since they are at lower intensities than those extracted from LV. Figure 5B shows the lipid profile of LV after background subtraction, which consists of 102 lipids from 14 different classes. We observed that many of the lipid subclasses shown to be enriched in the HIV envelope were also present in the manufactured LV samples including SM, ether PC, ether PE, PC, and PI species[15,16,18]. Cholesterol ester (CE), diacylglycerol (DG) and triacylglycerol (TG) species were still present in LV after the background subtraction step. These lipid classes are not typically known to be viral envelope

components. LPC and FA species are not previously known to be incorporated into the LV envelope, but were also observed after the background subtraction step in the LV lipid profile (Figure 5B) and were detected in the media from untransfected control cells (Figure 5C).. PC 16:1_18:2, which experienced a large decrease in abundance (FC=0.2) after LV production and increase after VSV G production in HEK 293T cells (Supporting Figure S8), was not detected in the concentrated LV samples. This suggests that this lipid is depleted in HEK 293T cells without incorporation into the LV envelope, possibly due to complex lipid remodeling processes to either maintain homeostasis during LV production or to provide fatty acid chains to other LV-envelope lipid species. The 16:1 alkyl chain was observed in some lipid species uniquely detected in LV, such as in PE 16:1_18:1 and as ether-linked chains in lipid species like EtherPC 16:1e_16:0, EtherPC 16:1e_18:1, EtherPE 16:1e_16:1, EtherPE 16:1e_20:1, EtherPE 16:1e_20:3, EtherPE 16:1e_22:3, EtherPE 16:1e_22:4 and EtherPE 18:2e_16:1 (Supporting Table S7). The 18:2 chain was less prominent in unique LV lipids, with the only instance of it being EtherPE 18:2e_16:1. CE 16:1, CE 18:2, PC 16:0_18:2 and EtherPE 18:2e_18:1 were detected in both the media blank and the LV sample. This suggests that remodeling processes may have resulted in both the 16:1 and 18:2 fatty acids being incorporated into the final LV product without PC 16:1_18:2 being directly incorporated into the LV envelope. Lipids with long poly-unsaturated chains (20:3, 20:4, 22:5, 22:6) from the PC, ether PC and ether PE lipid subclasses were detected in the LV sample, which are not found in previous studies of the HIV envelope[15,16,18]. Many lipids with short, saturated acyl chains, such as 14:0 and 16:0, were identified with significant fold changes in HEK 293T cells that had produced LV for 48 hr. However, only one instance of a 14:0-containing lipid species (EtherPC

16:0e_14:0) was detected in LV. Other lipid species from the PC, PE, PS and PI subclasses were detected with at least one 16:0 acyl chain. In addition to this, several ceramide-containing species, such as Cer_NS d18:1_16:0, SM d33:1, SM d34:1, SM d36:2, were detected in LV and experienced significant (FDR-adjusted $P<0.05$) fold changes in HEK 293T cells after 48 hr of LV production.

Concentrating LV using ultracentrifugation is rapid and requires minimal sample preparation. Alternative methods for isolating viruses include ultracentrifugation with sucrose or iodixanol gradients and detergent cushions[15,18,70]. The use of detergents complicates LCMS protocols and the reproducibility of sucrose or iodixanol gradients can be challenging, requiring specific technical skills; thus a single ultracentrifugation step proved optimal. By employing a data-driven blank subtraction method, the lipid profile of LV can be compared between different production conditions or different viral vector platforms in a straightforward manner. Using this strategy, hypotheses surrounding different aspects of LV production can be tested to improve our understanding of large-scale LV production for therapeutic use. 102 lipids were identified after subtracting the media background from the LV sample, 52% being unique to LV and of these, 79% representing phospholipids and sphingolipids (Figure 5C and Supporting Table S7). Of these lipids, 20 have $\log_2$ abundances >10 and may serve as potential quality assurance metrics or as target additives to increase the efficiency of LV production in biomanufacturing processes.

Conclusions

We have introduced a sensitive, rapid, reproducible, and high-throughput pipeline to measure the lipid profile of third generation LV and HEK 293T packaging cells. This workflow can be used as a tool to both understand the dynamics of producing LV at the large scales required for therapeutic doses and to monitor the LV lipid composition from a quality assurance standpoint. Rather than acquiring data using a data-dependent MSMS method for all injections, our pipeline uses MS-level scans solely for feature extraction to improve quantification and performs a smaller number of data dependent MSMS injections on pooled samples to simplify the feature annotation process. Using a targeted list of identified lipids and avoiding a full untargeted extraction on each sample reduces the complexity of the dataset, as typically <300 features are considered for all statistical analysis, compared to typical untargeted workflows, which extract thousands of features. This is increases efficiency when pre-processing raw LCMS data and facilitates any optimization to peak picking settings. VSV G expression was used as a control for lipid disruption due to extracellular vesicle release in HEK 293T cells and lipid fold changes with its expression correlated with the lipid dynamics arising due to LV production. Upon LV production, 148 lipid species in HEK 293T cells were found to experience significant (FDR-adjusted P<0.05) fold changes compared to controls. PC, SM, PI, ether PC, ether PE and ceramide species were impacted the most significantly, suggesting that these lipids are implicated in the production of LV and that they may serve as potential targets to increase biomanufacturing output. LV was isolated via ultracentrifugation and analyzed yielding 102 lipids, 53 being found only in LV. These lipids represent a valuable list of targets to further study from transduction efficiency and

quality assurance standpoints. These methods can be employed to reveal the lipid dynamics of clinical-grade LV production and enable targeted methods to quantify specific lipid components incorporated into final LV-based biotherapeutic formulations. These methods may also be translated to other viral vector platforms, such as Adeno-associated viral vectors, which are emerging as valuable lifesaving gene and cell therapy technologies.

Data Availability

Raw data files used in the article are deposited on MassIVE (University of California, San Diego: https://massive.ucsd.edu/ProteoSAFe/static/massive.jsp) as dataset number MSV000094299.

Conflicts of Interest

The authors declare no conflicts of interest.

Acknowledgements

J.C.S. and C.N.B. would like to gratefully acknowledge the Natural Sciences and Engineering Research Council of Canada, the Canadian Foundation for Innovation, the Ontario Research Fund and Carleton University for research funding. J.A.R. acknowledges the Ontario Graduate Scholarship program as well as Carleton University for internal scholarships. JS.D. gratefully acknowledge the Terry Fox Foundation for research funding.

Authors' Contributions

J.A.R. and J.A.M. were responsible for LCMS method development, data acquisition and data analysis. E.G. was responsible for cell culturing, sample preparation and lipid extractions. J.A.R. and E.G. were responsible for the experimental design. JS.D., C.N.B. and J.C.S. were responsible for funding the project and oversight of all activities. J.A.R. was responsible for writing the initial draft of the manuscript, and all co-authors contributed to editing and formatting the manuscript.

References

1 Wiley, Gene Therapy Clinical Trials Worldwide, https://a873679.fmphost.com/fmi/webd/GTCT, (accessed 17 March 2023).

2 J. Mátrai, M. K. Chuah and T. Vandendriessche, *Mol. Ther.*, 2010, **18**, 477–490.

3 C. Gándara, V. Affleck and E. A. Stoll, *Hum. Gene Ther. Methods*, 2018, **29**, 1–15.

4 S. Schuster, M. R. Bishop, C. Tam, E. K. Waller, P. Borchmann, J. McGuirk, U. Jäger, S. Jaglowski, C. Andreadis, J. Westin, I. Fleury, V. Bachanova, S. R. Foley, P. J. Ho, S. Mielke, J. M. Magenau, H. Holte, O. Anak, L. Pacaud, R. Awasthi, F. Tai, G. Salles and R. T. Maziarz, *Clin. Lymphoma Myeloma Leuk.*, 2017, **17**, S373–S374.

5 S. L. Maude, T. W. Laetsch, J. Buechner, S. Rives, M. Boyer, H. Bittencourt, P. Bader, M. R. Verneris, H. E. Stefanski, G. D. Myers, M. Qayed, B. De Moerloose, H. Hiramatsu, K. Schlis, K. L. Davis, P. L. Martin, E. R. Nemecek, G. A. Yanik, C. Peters, A. Baruchel, N. Boissel, F. Mechinaud, A. Balduzzi, J. Krueger, C. H. June, B. L. Levine, P. Wood, T. Taran, M. Leung, K. T. Mueller, Y. Zhang, K. Sen, D. Lebwohl, M. A. Pulsipher and S. A. Grupp, *N. Engl. J. Med.*, 2018, **378**, 439–448.

6 A. Shahryari, M. S. Jazi, S. Mohammadi, H. R. Nikoo, Z. Nazari, E. S. Hosseini, I. Burtscher, S. J. Mowla and H. Lickert, *Front. Genet.*, 2019, **10**, 1–25.

7 X. Wang and I. Rivière, *Mol. Ther. - Oncolytics*, 2016, **3**, 1–6.

8 F. L. Graham, J. Smiley, W. C. Russell and R. Nairn, *J. Gen. Virol.*, 1977, **36**, 59–72.

9 W. S. Pear, G. P. Nolan, M. L. Scott and D. Baltimore, *Proc. Natl. Acad. Sci. U. S. A.*, 1993, **90**, 8392–8396.

10 A. J. Valkama, H. M. Leinonen, E. M. Lipponen, V. Turkki, J. Malinen, T. Heikura, S. Ylä-Herttuala and H. P. Lesch, *Gene Ther.*, 2018, **25**, 39–46.

11 E. Palmer, C. Sporborg, A. Harrison, M. L. Martin and P. Feorino, *Arch. Virol.*, 1985, **85**, 189–196.

12 R. C. Aloia, F. C. Jensen, C. C. Curtain, P. W. Mobley and L. M. Gordon, *Lipid composition and fluidity of the human immunodeficiency virus*, 1988, vol. 85.

13 R. C. Aloia, H. Tian and F. C. Jensen, *Lipid composition and fluidity of the human immunodeficiency virus envelope and host cell plasma membranes*, 1993, vol. 90.

14 A. Ono and E. O. Freed, *Plasma membrane rafts play a critical role in HIV-1 assembly and release*, 2001, vol. 98.

15 B. Brügger, B. Glass, P. Haberkant, I. Leibrecht, F. T. Wieland and H. G. Kräusslich, *Proc. Natl. Acad. Sci. U. S. A.*, 2006, **103**, 2641–2646.

16 R. Chan, P. D. Uchil, J. Jin, G. Shui, D. E. Ott, W. Mothes and M. R. Wenk, *J. Virol.*, 2008, **82**, 11228–11238.

17 M. Lorizate, B. Brügger, H. Akiyama, B. Glass, B. Müller, G. Anderluh, F. T. Wieland and H. G. Kräusslich, *J. Biol. Chem.*, 2009, **284**, 22238–22247.

18 M. Lorizate, T. Sachsenheimer, B. Glass, A. Habermann, M. J. Gerl, H. G. Kräusslich and B. Brügger, *Cell. Microbiol.*, 2013, **15**, 292–304.

19 S. J. Blanksby and T. W. Mitchell, *Annu. Rev. Anal. Chem.*, 2010, **3**, 433–465.

20 M. Sud, E. Fahy, D. Cotter, A. Brown, E. A. Dennis, C. K. Glass, A. H. Merrill, R. C. Murphy, C. R. H. Raetz, D. W. Russell and S. Subramaniam, *Nucleic Acids*

Res., 2007, **35**, D527–D532.
21 T. Kind, K. H. Liu, D. Y. Lee, B. Defelice, J. K. Meissen and O. Fiehn, *Nat. Methods*, 2013, **10**, 755–758.
22 J. P. Koelmel, N. M. Kroeger, C. Z. Ulmer, J. A. Bowden, R. E. Patterson, J. A. Cochran, C. W. W. Beecher, T. J. Garrett and R. A. Yost, *BMC Bioinformatics*, 2017, **18**, 1–11.
23 A. Forest, M. Ruiz, B. Bouchard, G. Boucher, O. Gingras, C. Daneault, I. Robillard Frayne, D. Rhainds, J. C. Tardif, J. D. Rioux and C. Des Rosiers, *J. Proteome Res.*, 2018, **17**, 3657–3670.
24 P. T. Ivanova, S. B. Milne, M. O. Byrne, Y. Xiang and H. A. B. T.-M. in E. Brown, in *Lipidomics and Bioactive Lipids: Mass-Spectrometry–Based Lipid Analysis*, Academic Press, 2007, vol. 432, pp. 21–57.
25 J. C. Shon, S. M. Lee, J. H. Jung, Z. Wu, Y. S. Kwon, H. J. Sim and J. S. Seo, *Ecotoxicol. Environ. Saf.*, 2020, **202**, 110896.
26 P. Proitsi, M. Kim, L. Whiley, A. Simmons, M. Sattlecker, L. Velayudhan, M. K. Lupton, H. Soininen, I. Kloszewska, P. Mecocci, M. Tsolaki, B. Vellas, S. Lovestone, J. F. Powell, R. J. B. Dobson and C. Legido-Quigley, *Alzheimer's Dement.*, 2017, **13**, 140–151.
27 R. B. Chan, A. J. Perotte, B. Zhou, C. Liong, E. J. Shorr, K. S. Marder, U. J. Kang, C. H. Waters, O. A. Levy, Y. Xu, H. Bin Shim, I. Pe'Er, G. Di Paolo and R. N. Alcalay, *PLoS One*, 2017, **12**, e0172348–e0172348.
28 J. Wei, X. Li, L. Xiang, Y. Song, Y. Liu, Y. Jiang and Z. Cai, *J. Hazard. Mater.*, , DOI:10.1016/j.jhazmat.2019.121451.
29 C. Y. Hung, A. Chao, C. C. Wang, R. C. Wu, K. Y. Lu, H. Y. Lu, C. H. Lai and G. Lin, *Anal. Methods*, 2018, 10, 4970–4977.
30 X. Zhou, J. Mao, J. Ai, Y. Deng, M. R. Roth, C. Pound, J. Henegar, R. Welti and S. A. Bigler, *PLoS One*, , DOI:10.1371/journal.pone.0048889.
31 E. G. Bligh and W. J. Dyer, *Can. J. Biochem. Physiol.*, 1959, **37**, 911–917.
32 J. FOLCH, M. LEES and G. H. SLOANE STANLEY, *J. Biol. Chem.*, 1957, **226**, 497–509.
33 V. Matyash, G. Liebisch, T. V. Kurzchalia, A. Shevchenko and D. Schwudke, *J. Lipid Res.*, 2008, **49**, 1137–1146.
34 T. Cajka and O. Fiehn, *TrAC - Trends Anal. Chem.*, 2014, **61**, 192–206.
35 T. Cajka and O. Fiehn, *Metabolomics*, 2016, **12**, 1–11.
36 G. Liebisch, R. Ahrends, M. Arita, M. Arita, J. A. Bowden, C. S. Ejsing, W. J. Griffiths, M. Holčapek, H. Köfeler, T. W. Mitchell, M. R. Wenk and K. Ekroos, *Nat. Metab.*, 2019, 1, 745–747.
37 J. A. Bowden, A. Heckert, C. Z. Ulmer, C. M. Jones, J. P. Koelmel, L. Abdullah, L. Ahonen, Y. Alnouti, A. M. Armando, J. M. Asara, T. Bamba, J. R. Barr, J. Bergquist, C. H. Borchers, J. Brandsma, S. B. Breitkopf, T. Cajka, A. Cazenave-Gassiot, A. Checa, M. A. Cinel, R. A. Colas, S. Cremers, E. A. Dennis, J. E. Evans, A. Fauland, O. Fiehn, M. S. Gardner, T. J. Garrett, K. H. Gotlinger, J. Han, Y. Huang, A. H. Neo, T. Hyötyläinen, Y. Izumi, H. Jiang, H. Jiang, J. Jiang, M. Kachman, R. Kiyonami, K. Klavins, C. Klose, H. C. Köfeler, J. Kolmert, T. Koal, G. Koster, Z. Kuklenyik, I. J. Kurland, M. Leadley, K. Lin, K. R. Maddipati, D. McDougall, P. J. Meikle, N. A. Mellett, C. Monnin, M. A. Moseley, R. Nandakumar,

M. Oresic, R. Patterson, D. Peake, J. S. Pierce, M. Post, A. D. Postle, R. Pugh, Y. Qiu, O. Quehenberger, P. Ramrup, J. Rees, B. Rembiesa, D. Reynaud, M. R. Roth, S. Sales, K. Schuhmann, M. L. Schwartzman, C. N. Serhan, A. Shevchenko, S. E. Somerville, L. St John-Williams, M. A. Surma, H. Takeda, R. Thakare, J. W. Thompson, F. Torta, A. Triebl, M. Trötzmüller, S. J. K. Ubhayasekera, D. Vuckovic, J. M. Weir, R. Welti, M. R. Wenk, C. E. Wheelock, L. Yao, M. Yuan, X. H. Zhao and S. Zhou, *J. Lipid Res.*, 2017, **58**, 2275–2288.

38 T. Cajka, J. T. Smilowitz and O. Fiehn, *Anal. Chem.*, 2017, **89**, 12360–12368.

39 W. J. Bligh, E.G. and Dyer, *Can. J. Biochem. Physiol.*, 1959, **37**, 911–917.

40 F. Bonin, S. D. Ryan, L. Migahed, F. Mo, J. Lallier, D. J. Franks, H. Arai and S. A. L. Bennett, *J. Biol. Chem.*, 2004, **279**, 52425–52436.

41 V. Garcia, R. Krishnan, C. Davis, C. Batenchuk, F. Le Boeuf, H. Abdelbary and J. S. Diallo, *J. Vis. Exp*, 2014, 51890.

42 M. C. Chambers, B. MacLean, R. Burke, D. Amodei, D. L. Ruderman, S. Neumann, L. Gatto, B. Fischer, B. Pratt, J. Egertson, K. Hoff, D. Kessner, N. Tasman, N. Shulman, B. Frewen, T. A. Baker, M. Y. Brusniak, C. Paulse, D. Creasy, L. Flashner, K. Kani, C. Moulding, S. L. Seymour, L. M. Nuwaysir, B. Lefebvre, F. Kuhlmann, J. Roark, P. Rainer, S. Detlev, T. Hemenway, A. Huhmer, J. Langridge, B. Connolly, T. Chadick, K. Holly, J. Eckels, E. W. Deutsch, R. L. Moritz, J. E. Katz, D. B. Agus, M. MacCoss, D. L. Tabb and P. Mallick, *Nat. Biotechnol.*, 2012, **30**, 918–920.

43 R. Schmid, S. Heuckeroth, A. Korf, A. Smirnov, O. Myers, T. S. Dyrlund, R. Bushuiev, K. J. Murray, N. Hoffmann, M. Lu, A. Sarvepalli, Z. Zhang, M. Fleischauer, K. Dührkop, M. Wesner, S. J. Hoogstra, E. Rudt, O. Mokshyna, C. Brungs, K. Ponomarov, L. Mutabdžija, T. Damiani, C. J. Pudney, M. Earll, P. O. Helmer, T. R. Fallon, T. Schulze, A. Rivas-Ubach, A. Bilbao, H. Richter, L. F. Nothias, M. Wang, M. Orešič, J. K. Weng, S. Böcker, A. Jeibmann, H. Hayen, U. Karst, P. C. Dorrestein, D. Petras, X. Du and T. Pluskal, *Nat. Biotechnol.*, , DOI:10.1038/s41587-023-01690-2.

44 J. Yang, X. Zhao, X. Lu, X. Lin and G. Xu, *Front. Mol. Biosci.*, , DOI:10.3389/fmolb.2015.00004.

45 B. M. Bolstad, R. A. Irizarry, M. Åstrand and T. P. Speed, *Bioinformatics*, 2003, **19**, 185–193.

46 K. V. Ballman, D. E. Grill, A. L. Oberg and T. M. Therneau, *Bioinformatics*, 2004, **20**, 2778–2786.

47 B. A. Ejigu, D. Valkenborg, G. Baggerman, M. Vanaerschot, E. Witters, J. C. Dujardin, T. Burzykowski and M. Berg, *Omi. A J. Integr. Biol.*, 2013, **17**, 473–485.

48 B. Li, J. Tang, Q. Yang, X. Cui, S. Li, S. Chen, Q. Cao, W. Xue, N. Chen and F. Zhu, *Sci. Rep.*, 2016, **6**, 1–13.

49 R. Wei, J. Wang, M. Su, E. Jia, S. Chen, T. Chen and Y. Ni, *Sci. Rep.*, 2018, **8**, 1–10.

50 C. Lazar, T. Burger and S. Wieczorek, *imputeLCMD: A collection of methods for left-censored missing data imputation v. version 2.0 (2015).*, 2015.

51 X. Wang, M. Olszewska, J. Qu, T. Wasielewska, S. Bartido, G. Hermetet, M. Sadelain and I. Rivière, *J. Immunother.*, 2015, **38**, 127–135.

52 W. Barczak, W. Suchorska, B. Rubiś and K. Kulcenty, *Mol. Biotechnol.*, 2014, **57**,

195–200.
53 J. S. McDougal, S. P. Cort, M. S. Kennedy, C. D. Cabridilla, P. M. Feorino, D. P. Francis, D. Hicks, V. S. Kalyanaraman and L. S. Martin, *J. Immunol. Methods*, 1985, **76**, 171–183.
54 D. S. Healey, W. J. Maskill, E. V. Neate, F. Beaton and I. D. Gust, *J. Virol. Methods*, 1988, **20**, 115–125.
55 O. W. Merten, M. Hebben and C. Bovolenta, *Mol. Ther. - Methods Clin. Dev.*, 2016, **3**, 16017.
56 C. Breil, M. Abert Vian, T. Zemb, W. Kunz and F. Chemat, *Int. J. Mol. Sci.*, 2017, **18**, 2–21.
57 A. C. Schrimpe-Rutledge, S. G. Codreanu, S. D. Sherrod and J. A. McLean, *J. Am. Soc. Mass Spectrom.*, 2016, **27**, 1897–1905.
58 J. Koelmel, M. Sartain, J. Salcedo, A. Murali, X. Li and S. Stow, *Agil. Technol. Appl. Note*, 2019, **5994**–**0775E**, 1–10.
59 M. Baker, *Nat. Methods*, 2011, **8**, 117–121.
60 T. Välikangas, T. Suomi and L. L. Elo, *Brief. Bioinform.*, 2018, **19**, 1–11.
61 J. Yang, X. Zhao, X. Lu, X. Lin and G. Xu, *Front. Mol. Biosci.*, 2015, **2**, 1–9.
62 G. Paglia, A. J. Smith and G. Astarita, *Mass Spectrom. Rev.*, 2022, **41**, 722–765.
63 V. Davies, J. Wandy, S. Weidt, J. J. J. Van Der Hooft, A. Miller, R. Daly and S. Rogers, *Anal. Chem.*, 2021, **93**, 5676–5683.
64 A. Jeucken and J. F. Brouwers, *Biomolecules*, 2019, **9**, 1–14.
65 H. C. Leier, J. B. Weinstein, J. E. Kyle, J. Y. Lee, L. M. Bramer, K. G. Stratton, D. Kempthorne, A. R. Navratil, E. G. Tafesse, T. Hornemann, W. B. Messer, E. A. Dennis, T. O. Metz, E. Barklis and F. G. Tafesse, *Nat. Commun.*, 2020, **11**, 1–15.
66 C. Meyer, J. Losacco, Z. Stickney, L. Li, G. Marriott and B. Lu, *Int. J. Nanomedicine*, 2017, **12**, 3153–3170.
67 H. M. van Dongen, N. Masoumi, K. W. Witwer and D. M. Pegtel, *Microbiol. Mol. Biol. Rev.*, 2016, **80**, 369–386.
68 P. E. Mangeot, S. Dollet, M. Girard, C. Ciancia, S. Joly, M. Peschanski and V. Lotteau, *Mol. Ther.*, 2011, **19**, 1656–1666.
69 J. L. Cleary, G. T. Luu, E. C. Pierce, R. J. Dutton and L. M. Sanchez, *J. Am. Soc. Mass Spectrom.*, 2019, **30**, 1426–1434.
70 R. Welker, H. Hohenberg, U. Tessmer, C. Huckhagel and H.-G. Kräusslich, *J. Virol.*, 2000, **74**, 1168–1177.

Contact Information

J. A. Roberts: joshuaroberts@cmail.carleton.ca

E. Godbout: elgodbout@ohri.ca

C. N. Boddy: Christopher.Boddy@uottawa.ca

J-S Diallo: jsdiallo@ohri.ca

J. C. Smith: jeff.smith@carleton.ca